

# Inelastic surface deformation during the 2013 $M_w$ 7.7 Balochistan, Pakistan, earthquake

A. Vallage<sup>1\*</sup>, Y. Klinger<sup>1</sup>, R. Grandin<sup>1</sup>, H.S. Bhat<sup>1</sup>, and M. Pierrot-Deseilligny<sup>2</sup>

<sup>1</sup>Institut de Physique du Globe de Paris, Sorbonne Paris Cité, Université Paris Diderot, UMR 7154 CNRS, 1 Rue Jussieu, F-75005 Paris, France

<sup>2</sup>IGN, LOEMI, Université Paris-Est, 73 Avenue de Paris, 94165 Saint-Mandé cedex, France

## ABSTRACT

Comprehensive quantification of the near-field deformation associated with an earthquake is difficult due to the inherent complexity of surface ruptures. The A.D. 2013  $M_w$  7.7 Balochistan (Pakistan) earthquake, dominated by left-lateral motion with some reverse component, ruptured a 200-km-long section of the Hoshab fault. We characterize the coseismic rupture in detail along its entire length. Optical and radar satellite images are combined to derive the full three-dimensional far-field displacement (115 m pixel size) and the high-resolution 2.5 m pixel horizontal displacement field resulting from the earthquake. We show that the vertical deformation is significant in several locations. The high-resolution near-field horizontal displacement (<1 km around the rupture) reveals inelastic shortening at the fault surface significantly larger than expected from simple elastic modeling. A zone of extension in the hanging wall, as much as 1 km wide, concentrating numerous tensile cracks visible in submeter-scale optical images, compensates for this excess shortening.

## INTRODUCTION

Accurate quantification of deformation along earthquake surface ruptures can be difficult due to complexity of the rupture geometry (Klinger et al., 2005; Milliner et al., 2015). When available, detailed ground surface measurements show that surface-slip variations often correlate with geometrical complexities of the surface rupture (Klinger et al., 2006; Klinger, 2010; Wei et al., 2011), distributing coseismic slip through partitioned (Bowman et al., 2003; King et al., 2005) or distributed deformation (Vallage et al., 2014). Effects due to interaction between an upward-propagating rupture and the free surface could also add complexity to the surface rupture (Madariaga, 2003). Even so, surface slip distributions are commonly used to estimate earthquake magnitude (e.g., Wells and Coppersmith, 1994). The apparent discrepancy between slip modeled at depth and slip observed at the surface led some researchers to propose that continental earthquake ruptures are characterized by some shallow-slip deficit related to fault maturity and local sediment thickness (Fialko et al., 2005; Dolan and Haravitch, 2014; Zinke et al., 2014).

On 24 September 2013, the  $M_w$  7.7 Balochistan earthquake ruptured 200 km of the Hoshab fault in Pakistan (Avouac et al., 2014; Barnhart et al., 2014, 2015; Gold et al., 2015; Jolivet et al., 2014; Zhou et al., 2015; Zinke et al., 2014). Although the rupture propagated bilaterally on a curved, north-dipping fault ( $45^\circ$ – $75^\circ$ ) with azimuth veering from  $N200^\circ$  to  $N240^\circ$ , the earthquake is mostly characterized by left-lateral strike slip, with a limited reverse component.

Using 15 m Landsat-8, 2.5 m SPOT-5, Google Earth™ submeter-scale optical images, and TerraSAR-X radar data, we reconstructed the full three-dimensional (3-D) displacement field and the high-resolution displacement field to characterize the near-field deformation along the entire rupture. The rupture trace was also mapped in detail.

## MEASUREMENT OF SURFACE DISPLACEMENT FIELD

Figure 1 shows the 2.5 m pixel size horizontal displacement field derived from correlation of preearthquake and postearthquake SPOT-5 satellite images using MicMac (Rosu et al., 2015; <http://logiciels.ign.fr/?-Micmac,3->), af-

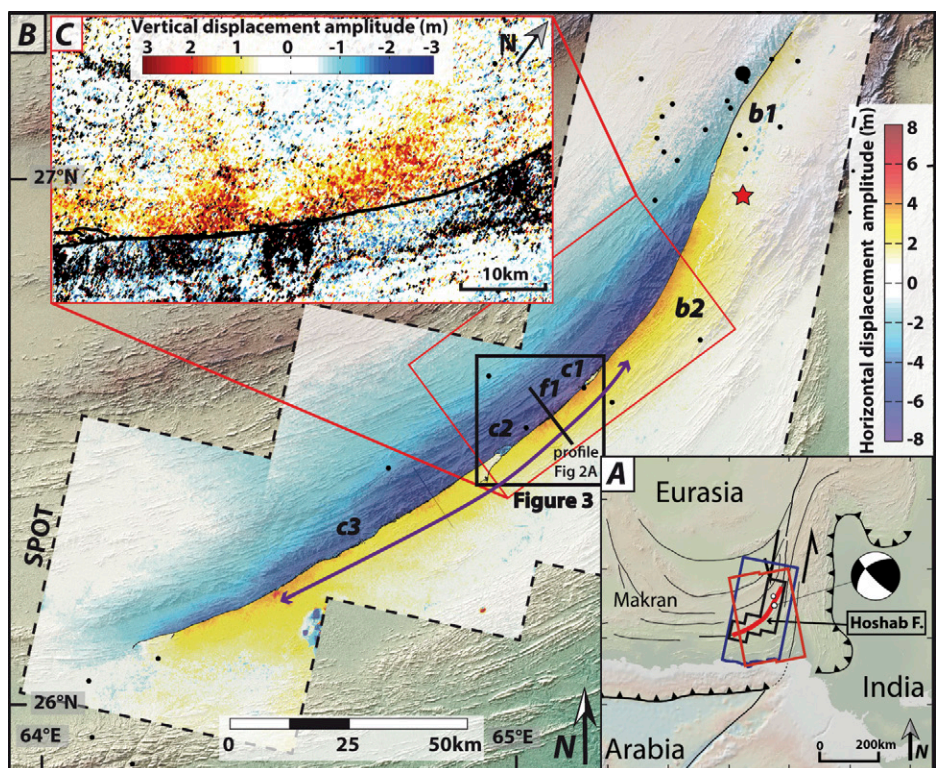


**Figure 1.** A: A.D. 2013  $M_w$  7.7 Balochistan (Pakistan) rupture along the Hoshab fault (F), which is part of the Makran subduction accretionary wedge (after Avouac et al., 2014). SPOT-5 (black), Landsat-8 (blue), and TerraSAR-X (red) image swaths are indicated. B: 2.5 m pixel horizontal displacement field from correlation of preevent and postevent SPOT-5 images. Amplitude of displacement is negative for westward motion. Main geometrical asperities, bends b1 and b2, relay zones c1 and c2, and paired bend c3, f1, and the area of distributed deformation (purple arrow) are indicated along rupture. Topography from 30 m pixel ASTER (Advanced Spaceborne Thermal Emission and Reflection Radiometer) digital elevation model. Epicenter (star) and 3 first months of aftershocks (dots) are from the U.S. Geological Survey. C: Extract of the vertical displacement field showing uplift in the southern part of the rupture.

\*E-mail: vallage@ipgp.fr

ter coregistration and orthorectification using COSI-Corr (Leprince et al., 2007; [http://www.tectonics.caltech.edu/slipp\\_history/spot\\_coseis/](http://www.tectonics.caltech.edu/slipp_history/spot_coseis/)) (for image processing methodologies, see the GSA Data Repository<sup>1</sup>). The displacement field has been flattened to zero far from the rupture. North of the epicenter, the total horizontal displacement across the rupture remains  $<4$  m. Conversely, the horizontal displacement increases quickly southward, reaching 14 m in the central southern part. Due to the northwestward fault dip, the distribution of horizontal motion is asymmetric, with more displacement north of the fault. Slip affects a 10 km narrow band in the footwall, with ground displacements to 5.5 m, and a broader band of 20–25 km in the hanging wall, with the displacement peaking at 8.5 m.

The high-resolution displacement field derived from the SPOT-5 imagery allows the recognition of several geometrical complexities at different scales. At large scale, two bends, b1 and b2 (Fig. 1), characterize the overall geometry of the fault. Although b1 does not affect the deformation pattern significantly, b2 has a strong signature in the horizontal displacement field. Bend b2, where the rupture starts to veer toward the southwest with a shallower dip angle, corresponds to the area of maximum horizontal deformation. South of these two large-scale complexities, several features, kilometers in size, are identifiable: two relay zones, c1 and c2, and a paired bend, c3. Smaller scale (hundreds of meters) features, such as f1, corresponding to successions of sharp bends and en echelon cracks, are also found in many places. Although the rupture propagated along a long-lived thrust structure, most of these geometrical asperities relate to local azimuth deviation from the main thrust azimuth.

The horizontal displacement was combined with TerraSAR-X radar line-of-sight displacement to derive the vertical deformation (see the Data Repository), with a ground resolution of 115 m (Fig. 1C; Fig. DR2 in the Data Repository). Vertical motion is almost zero in the northern part of the rupture, where the fault strikes  $\sim$ N200°. South of bend b2, however, up to 4 m of coseismic relative vertical displacement is accommodated across the fault, mostly due to uplift of the hanging wall (Zhou et al., 2015).

## NEAR-FIELD CHARACTERIZATION OF THE RUPTURE

The continuous 2.5-m-resolution horizontal displacement field allows for mapping details of the deformation pattern due to the 2013 event. Figure 2A shows a fault-normal shortening

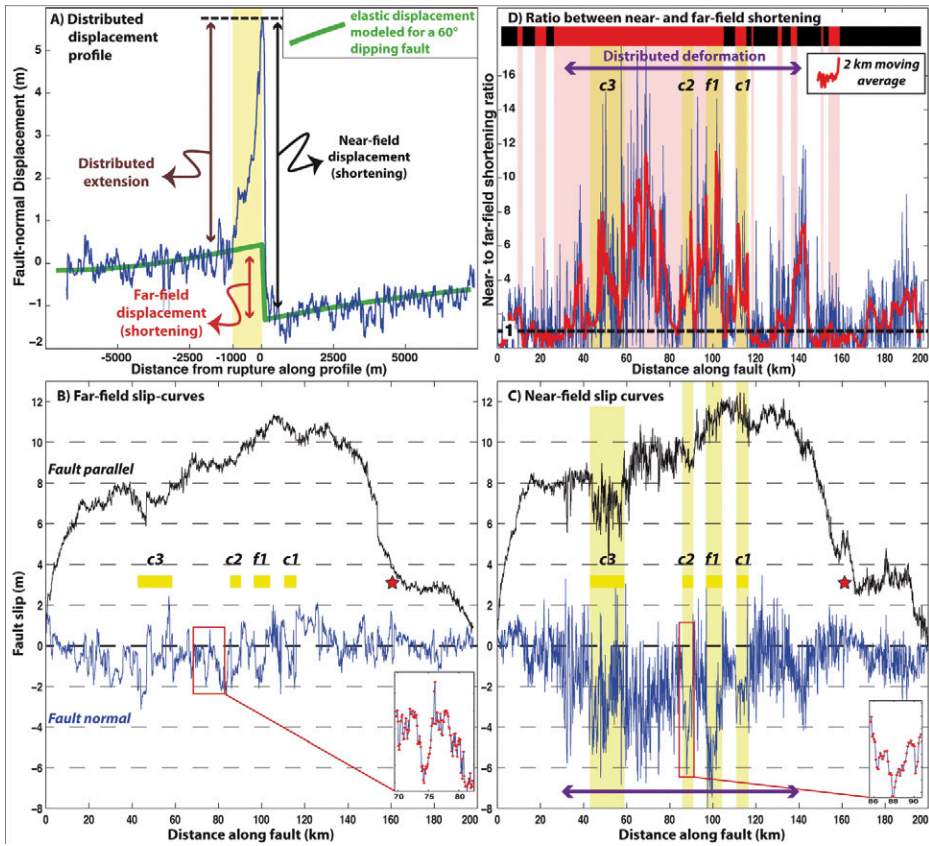


**Figure 2.** A: Fault-normal displacement profile (in blue) from 15-km-long and 100-m-wide stack, showing large shortening at the fault, balanced by extension over ~1 km in the hanging wall. Elastic modeling (in green) does not fit near-field deformation, although it reproduces well the far-field pattern. B: Fault-parallel (black) and fault-normal (blue) slip curves derived from 2000 far-field measurements (inset shows measured density). Negative values of fault-normal displacements indicate shortening. Yellow boxes indicate locations of asperities. Star corresponds to U.S. Geological Survey epicenter. C: Same as in B, for near-field measurements. Purple arrow shows zone where near-field and far-field fault-normal displacements differ significantly. D: Ratio between near-field and far-field shortening in blue, with 2 km average in red. The ratio is well above 1 in zones of distributed deformation, including main geometrical complexities, also corresponding to missing slip zones (red in the upper bar) identified by Zinke et al. (2014).

profile (blue curve: stack in a 15-km-long and 100-m-wide box) along the direction perpendicular to the local azimuth of the rupture. This kind of profile is observed in many locations along the southern part of the rupture. For the section located 1 km away or more (herein referred to as far field) from the actual ground rupture, the shape and amplitude of displacement are generally consistent with an elastic dislocation dipping 60° to the north (green curve in Fig. 2A; modeled after Okada, 1992), in agreement with geophysical inversions (Avouac et al., 2014; Barnhart et al., 2014; Jolivet et al., 2014). Conversely, the section of the hanging wall located directly next to the ground rupture shows an excess of shortening incompatible with simple elastic deformation. Because near-field (0.1–1 km north of the scarp) and far-field (>1 km away from the scarp) deformation need to be reconciled eventually, a zone of distributed extension located in the hanging wall compensates for the extra shortening. In that case, the total

relative extension in the hanging wall reaches 4.5 m, over a width of 1 km (Fig. 2A).

In order to assess the along-strike extent of this inelastic deformation in the hanging wall, we systematically measured far-field and near-field displacement on 2000 independent profiles (100-m-wide stacks located every 100 m). For each profile, we measured both the fault-parallel (left-lateral motion positive) and the fault-normal (shortening negative) displacement. Overall, the far-field displacement distribution (Fig. 2B) is in good agreement, both in amplitude and spatial variations, with previously published strike-slip distributions (Avouac et al., 2014; Barnhart et al., 2015; Gold et al., 2015; Zhou et al., 2015; Zinke et al., 2014), yielding an averaged total slip amplitude of 7.3 m, with a maximum of 11.5 m. Despite a significant change of azimuth along strike, strike-slip motion dominates until the end of the rupture, with shortening  $<3$  m. Displacements measured in the near field are slightly larger, due to attenuation

<sup>1</sup>GSA Data Repository item 2015360, optical image and InSAR processing methodology, and Figures DR1 and DR2, is available online at [www.geosociety.org/pubs/ft2015.htm](http://www.geosociety.org/pubs/ft2015.htm), or on request from editing@geosociety.org or Documents Secretary, GSA, P.O. Box 9140, Boulder, CO 80301, USA.

of elastic displacement with distance (Okada, 1992), with an average total surface slip of 8 m and a maximum of 14 m (Fig. 2C). Near-field fault-normal surface slip, however, shows pronounced differences in amplitude when compared to far-field measurements, locally reaching 6–7 m in shortening. Differences between the near-field and far-field shortening measurements are mostly located along a 110-km-long zone (purple arrow from km 30 to km 140 in Figs. 1, 2C, and 2D) previously identified as missing slip areas (identified in red in top bar of Fig. 2D) by Zinke et al. (2014) based on analyses of geomorphic marker offsets. The lateral slip variability is also larger along this section of the fault, with significant variations occurring both on the fault-parallel and the fault-normal components over only a few kilometers (Fig. 2C). In some of the mapped complex rupture zones (relay zone c2 and paired bend c3; Fig. 2C) the two components are anticorrelated in amplitude with an increase in the fault-normal component when the fault-parallel component decreases. The density of measurements and spatial coherence ensure that this signal is real. These local matches between slip variation and ground-rupture complexity are interpreted as the signature of the fault structure complexity, possibly related to lateral segmentation (Klinger et al., 2006; Wesnousky, 2008; Klinger, 2010). Nevertheless, as the ratio between the near-field and far-field shortening is well above 1 (Fig. 2D) over a 110-km-long zone, it suggests that there is another process at a larger scale. Figure 3 shows an along-strike succession of wide damaged zones, indicated by the pink color where the displacement is mostly perpendicular to fault azimuth, alternating with sections where deformation is more localized, with a sharper transition from yellow to blue indicative of dominant fault-parallel motion. Using submeter-scale optical imagery (Worldview, SPOT-5, and Google Earth), we mapped the entire surface rupture at 1:500 scale, down to decimeter-scale cracks. Damage zones (Gold et al., 2015; Zinke et al., 2014) are characterized by a band of subparallel tensile cracks that spread across the hanging wall, away from the frontal scarp, over distances from a few hundred meters to 1 km. Figure 3B shows the extent of cracking in the hanging wall inside zone f1, affecting the entire sedimentary wedge located between the frontal thrust and the basement outcrop in the background. It is representative of the deformation occurring along the entire length of the distributed deformation zone. The relatively flat topography of the affected area rules out landsliding as a primary cause of cracking. The frontal scarp, which carries most of the shortening, remains very localized and zigzags at the scale of hundreds of meters following local topography. Therefore, it suggests that the thrust fault flattens to a shallow dip when it reaches the surface. In contrast, the

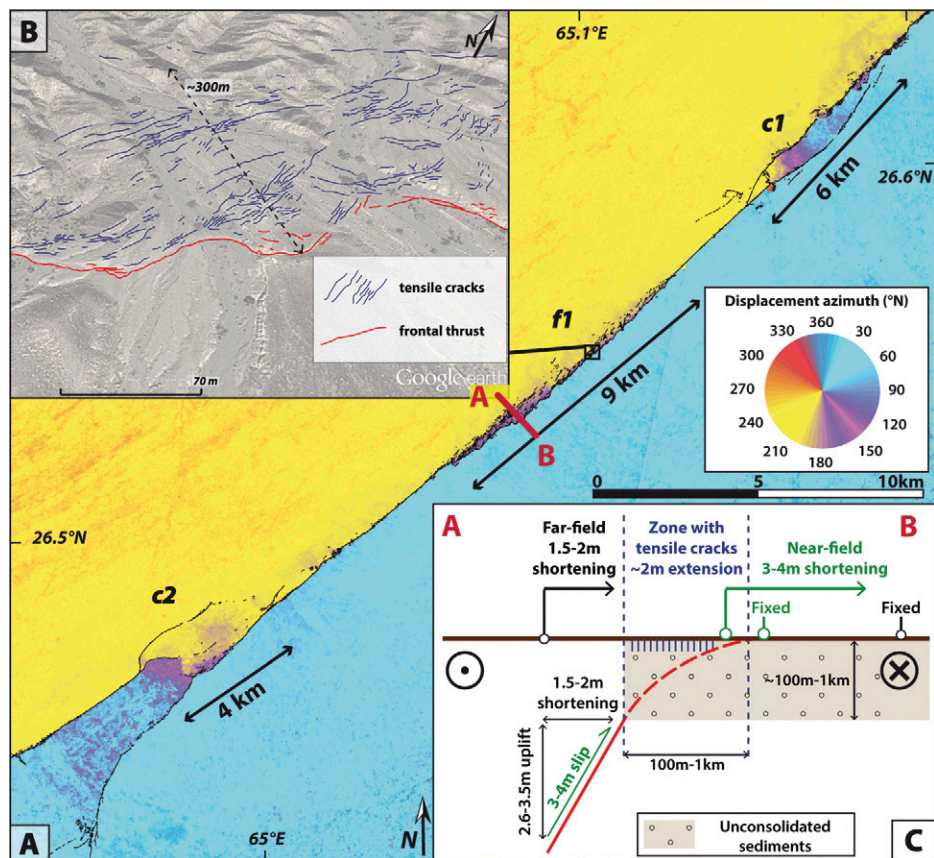


**Figure 3.** A: Detailed mapping of surface ruptures from optical images in a zone of distributed deformation, delimited by relay zones c1 and c2. Areas where shortening perpendicular to the rupture dominates are indicated in pink, which corresponds to highly distributed deformation. B: Submeter-scale optical image showing tensile cracks in the hanging wall of the localized frontal thrust. Local azimuth of the thrust varies according to local topography; strike-slip motion is distributed over the entire structure. C: Idealized cross section at the Figure 2A profile location, illustrating the full transfer of slip from depth to the frontal scarp along with significant extension in the hanging wall (see discussion in text).

strike-slip component does not always localize at the front and instead is distributed over the entire zone of cracking, together with the opening component, making direct measurement of the strike-slip on images (Gold et al., 2015) or in the field difficult. Our measurements show that eventually the total budget of displacement is taken up by the numerous distributed cracks activated by the rupture.

## CONCLUSIONS

Figure 3C shows an idealized cross section that reconciles far-field and near-field measurements along the 110-km-long section where we found excess shortening at the fault. Restoration of the 3-D far-field displacements on an averaged 60° north-dipping fault indicates that ~3–4 m of reverse slip took place at depth on the fault plane (Avouac et al., 2014; Barnhart et al., 2014; Jolivet et al., 2014). Such slip would project at the surface into 1.5–2 m of horizontal shortening and ~3 m of uplift, but could not account for the 3–4 m of horizontal shortening that we measured in the near field, directly at the rupture tip. We suggest that this apparent

excess of shortening at the surface results from flattening of the fault when it reaches the free surface. This interpretation assumes that the total amount of slip on the fault plane remains constant as the rupture propagates updip, explaining the local increase of the shortening at the surface tip of the rupture. It is likely that deformation related to surficial fault geometry is also enhanced by the effect of the propagating rupture encountering the free surface (Gabuchian et al., 2014; Madariaga, 2003; Oglesby et al., 2000), as suggested by large deformation observed in the hanging wall of the A.D. 2011 Tohoku-Oki (Japan) earthquake (Fujiwara et al., 2011; Kodaira et al., 2012).

Such a change in geometry promotes extension in the hanging wall that is in turn accommodated by the distributed set of tensile cracks observed on images. This interpretation is supported by the observation that, although widespread along the 110-km-long section, the excess shortening feature seems to be found mostly in locations where the rupture propagated at least at a few hundred meters away from the front of the folded basement, through

surficial unconsolidated sediments (Zinke et al., 2014). We suggest that this distributed deformation results from the oblique mode of rupture, because it is only observed where significant thrusting occurs in addition to strike slip, or in geometric complexities, as pointed out by Milliner et al. (2015).

As near-fault distributed deformation becomes measurable thanks to high-resolution imagery, comparison with broader scale geodetic data (GPS and interferometric synthetic aperture radar) may suggest that actual shallow slip deficit (Fialko et al., 2005) during very large earthquakes may be the exception rather than the rule.

## ACKNOWLEDGMENTS

Numerical computations were performed on the S-CAPAD platform, Institut de Physique du Globe de Paris (IPGP), France. This work was supported by Agence National de la Recherche (ANR) GeoS-MEC contract ANR-12-BS06-0016, and the Centre National d'Études Spatiales (CNES) TOSCA ISIS programs. We thank B. Holdsworth, J. Hollingsworth, and three anonymous reviewers for insightful comments. This is IPGP contribution #3689.

## REFERENCES CITED

Avouac, J.P., Ayoub, F., Wei, S., Ampuero, J.P., Meng, L., Leprince, S., Jolivet, R., Duputel, Z., and Helmberger, D., 2014, The 2013, Mw 7.7 Balochistan earthquake, energetic strike-slip reactivation of a thrust fault: *Earth and Planetary Science Letters*, v. 391, p. 128–134, doi:10.1016/j.epsl.2014.01.036.

Barnhart, W.D., Hayes, G.P., Briggs, R.W., Gold, R.D., and Bilham, R., 2014, Ball-and-socket tectonic rotation during the 2013 Mw 7.7 Balochistan earthquake: *Earth and Planetary Science Letters*, v. 403, p. 210–216, doi:10.1016/j.epsl.2014.07.001.

Barnhart, W.D., Briggs, R.W., Reitman, N.G., Gold, R.D., and Hayes, G.P., 2015, Evidence for slip partitioning and bimodal slip behavior on a single fault: Surface slip characteristics of the 2013 Mw 7.7 Balochistan, Pakistan earthquake: *Earth and Planetary Science Letters*, v. 420, p. 1–11, doi:10.1016/j.epsl.2015.03.027.

Bowman, D., King, G., and Tapponnier, P., 2003, Slip partitioning by elastoplastic propagation of oblique slip at depth: *Science*, v. 300, p. 1121–1123, doi:10.1126/science.1082180.

Dolan, J.F., and Haravitch, B.D., 2014, How well do surface slip measurements track slip at depth in large strike-slip earthquakes? The importance of fault structural maturity in controlling on-fault slip versus off-fault surface deformation: *Earth and Planetary Science Letters*, v. 388, p. 38–47, doi:10.1016/j.epsl.2013.11.043.

Fialko, Y., Sandwell, D., Simons, M., and Rosen, P., 2005, Three-dimensional deformation caused by the Bam, Iran, earthquake and the origin of shallow slip deficit: *Nature*, v. 435, p. 295–299, doi:10.1038/nature03425.

Fujiwara, T., Kodaira, S., No, T., Kaiho, Y., Takahashi, N., and Kaneda, Y., 2011, The 2011 Tohoku-Oki earthquake: Displacement reaching the trench axis: *Science*, v. 334, p. 1240, doi:10.1126/science.1211554.

Gabuchian, V., Rosakis, A.J., Lapusta, N., and Oglesby, D.D., 2014, Experimental investigation of strong ground motion due to thrust fault earthquakes: *Journal of Geophysical Research*, v. 119, p. 1316–1336, doi:10.1002/2013JB010409.

Gold, R.D., Reitman, N.G., Briggs, R.W., Barnhart, W.D., Hayes, G.P., and Wilson, E., 2015, On- and off-fault deformation associated with the September 2013  $M_w$  7.7 Balochistan earthquake: Implications for geologic slip rate measurements: *Tectonophysics*, doi:10.1016/j.tecto.2015.08.019.

Jolivet, R., et al., 2014, The 2013 Mw 7.7 Balochistan earthquake: Seismic potential of an accretionary wedge: *Seismological Society of America Bulletin*, v. 104, p. 1020–1030, doi:10.1785/0120130313.

King, G., Klinger, Y., Bowman, D., and Tapponnier, P., 2005, Slip partitioned surface breaks for the 2001 Kokoxili earthquake, China (Mw 7.8): *Seismological Society of America Bulletin*, v. 95, p. 731–738, doi:10.1785/0120040101.

Klinger, Y., 2010, Relation between continental strike-slip earthquake segmentation and thickness of the crust: *Journal of Geophysical Research*, v. 115, B07306, doi:10.1029/2009JB006550.

Klinger, Y., Xu, X.W., Tapponnier, P., Van der Woerd, J., Lasserre, C., and King, G., 2005, High-resolution satellite imagery mapping of the surface rupture and slip distribution of the MW 7.8, 14 November 2001 Kokoxili earthquake, Kunlun fault, northern Tibet, China: *Seismological Society of America Bulletin*, v. 95, p. 1970–1987, doi:10.1785/0120040233.

Klinger, Y., Michel, R., and King, G.C.P., 2006, Evidence for an earthquake barrier model from Mw similar to 7.8 Kokoxili (Tibet) earthquake slip-distribution: *Earth and Planetary Science Letters*, v. 242, p. 354–364, doi:10.1016/j.epsl.2005.12.003.

Kodaira, S., No, T., Nakamura, Y., Fujiwara, T., Kaiho, Y., Miura, S., Takahashi, N., Kaneda, Y., and Taira, A., 2012, Coseismic fault rupture at the trench axis during the 2011 Tohoku-oki earthquake: *Nature Geoscience*, v. 5, p. 646–650, doi:10.1038/ngeo1547.

Leprince, S., Barbot, S., Ayoub, F., and Avouac, J.P., 2007, Automatic and precise orthorectification, coregistration, and subpixel correlation of satellite images, application to ground deformation measurements: *IEEE Transactions on Geoscience and Remote Sensing*, v. 45, p. 1529–1558, doi:10.1109/TGRS.2006.888937.

Madariaga, R., 2003, Radiation from a finite reverse fault in a half space: *Pure and Applied Geophysics*, v. 160, p. 555–577, doi:10.1007/PL00012550.

Milliner, C.W.D., Dolan, J.F., Hollingsworth, J., Leprinse, S., Ayoub, F., and Sammis, C.G., 2015, Quantifying near-field and off-fault deformation patterns of the 1992 Mw7.3 Landers earthquake: *Geochemistry, Geophysics, Geosystems*, v. 16, p. 1577–1598, doi:10.1002/2014GC005693.

Oglesby, D.D., Archuleta, R.J., and Nielsen, S.B., 2000, The three-dimensional dynamics of dipping faults: *Seismological Society of America Bulletin*, v. 90, p. 616–628, doi:10.1785/0119990113.

Okada, Y., 1992, Internal deformation due to shear and tensile faults in a half-space: *Seismological Society of America Bulletin*, v. 82, p. 1018–1040.

Rosu, A.-M., Pierrot-Deseilligny, M., Delorme, A., Binet, R., and Klinger, Y., 2015, Measurement of ground displacement from optical satellite image correlation using the free open-source software MicMac: *ISPRS Journal of Photogrammetry and Remote Sensing*, v. 100, p. 48–59, doi:10.1016/j.isprsjprs.2014.03.002.

Vallage, A., Deves, M.H., Klinger, Y., King, G.C.P., and Ruppert, N.A., 2014, Localized slip and distributed deformation in oblique settings: The example of the Denali fault system, Alaska: *Geophysical Journal International*, v. 197, p. 1284–1298, doi:10.1093/gji/ggu100.

Wei, S., et al., 2011, Surficial simplicity of the 2010 El Mayor–Cucapah earthquake of Baja California in Mexico: *Nature Geoscience*, v. 4, p. 615–618, doi:10.1038/ngeo1213.

Wells, D.L., and Coppersmith, K.J., 1994, New empirical relationships among magnitude, rupture length, rupture width, rupture area, and surface displacement: *Seismological Society of America Bulletin*, v. 84, p. 974–1002.

Wesnousky, S., 2008, Displacement and geometrical characteristics of earthquake surface ruptures: Issues and implications for seismic-hazard analysis and the process of earthquake rupture: *Seismological Society of America Bulletin*, v. 98, p. 1609–1632, doi:10.1785/0120070111.

Zhou, Y., Elliot, J.R., Parsons, B., and Walker, R.T., 2015, The 2013 Balochistan earthquake: An extraordinary or completely ordinary event?: *Geophysical Research Letters*, v. 42, p. 6236–6243, doi:10.1002/2015GL065096.

Zinke, R., Hollingsworth, J., and Dolan, J.F., 2014, Surface slip and off-fault deformation patterns in the 2013 MW7.7 Balochistan, Pakistan earthquake: Implications for controls on the distribution of near-surface coseismic slip: *Geochemistry, Geophysics, Geosystems*, v. 15, p. 5034–5050, doi:10.1002/2014GC005538.

Manuscript received 24 August 2015

Revised manuscript received 12 October 2015

Manuscript accepted 14 October 2015

Printed in USA